Desalination and Water Treatment
www.deswater.com

doi: 10.5004/dwt.2018.22282

121 (2018) 53–64
July

Adsorption studies of amine-modified green synthesized Fe_3O_4 nanoparticles for the removal of nickel from aqueous solution

G. Gopika[a], K. Nithya[b,*], Asha Sathish[a]

[a]*Department of Sciences, Amrita School of Engineering, Amrita Vishwa Vidyapeetham, Coimbatore, Tamil Nadu, India, Tel. +8547165758; email: gopikag141995@gmail.com (G. Gopika), Tel. +9943977361; email: s_asha@cb.amrita.edu (A. Sathish)*
[b]*Dept. of Chemical Engineering and Materials Science, Amrita School of Engineering, Amrita Vishwa Vidyapeetham, Coimbatore, Tamil Nadu, India, Tel. +91 9443477623; email: nithiamrita@gmail.com*

Received 22 February 2018; Accepted 28 March 2018

ABSTRACT

The magnetite nanoparticles were synthesized through co-precipitation method and were coated with neem (*Azadirachta indica*) leaf extract. The adsorbent was further modified by the addition of ethylene diamine for better performance. The synthesized material was characterized by Fourier transform infrared spectroscopy, scanning electron microscopy, Energy dispersive X-ray spectroscopy, thermo gravimetric analysis and X-ray diffraction techniques. Parameters influencing the adsorption such as concentration, temperature, pH, contact time and dosage were optimized through batch studies. Isotherm studies were conducted by plotting and analyzing the Langmuir, Freundlich and Dubinin–Radushkevich isotherm models. The pseudo-first and pseudo-second order kinetic studies were carried out to understand the reaction kinetics. The adsorption was found to be efficient at room temperature with a pH of 6. The optimum dosage of adsorbent was found to be 0.2 g and the reaction attained equilibrium in 90 min. The maximum adsorption capacity of the material was found to be 19.23 mg/g from the Langmuir isotherm model. The temperature studies exhibit the reaction to be exothermic in nature. An appreciable desorption of the metal ions was obtained using 0.8 N HCl and the efficiency was found to be 79%.

Keywords: Magnetite; Ethylene diamine; Adsorption; Nickel; Desorption

1. Introduction

The extent of industrialization has increased into a very large extent in recent years. So has increased its effects on the ecosystem. A large number of water bodies across the world are severely polluted by industrial effluents which are discharged into water bodies without proper treatment. Heavy metals are one among the most common industrial pollutants. A metal whose density exceeds 5 g/cc can be categorized as a heavy metal [1]. These metals can either be present as cations or oxyanions. There are chances for these metal ions to get accumulated in the body of living organisms and thereby causing toxic effects. Nickel is one among the heavy metals found in the industrial wastewaters which is majorly found in the form of Ni(II) ions. Nickel finds extensive application in industries such as batteries, alloys, machineries, electroplating, petroleum, construction and certain household appliances. The Ministry of Environment and Forests, Government of India, has suggested a value of 3 mg/L or lower as the Ni(II) ions permissible concentrations in industrial effluents [2]. Long-term exposure to Ni(II) ions can cause liver and kidney damage, lung cancer, dermatitis, nausea, vomiting, renal edema, hair loss, chronic asthma, etc. [3,4].

The conventional methods that exist for metal ion removal such as ion exchange, ultra filtration, chemical precipitation

---

* Corresponding author.

Presented at the 3rd International Conference on Recent Advancements in Chemical, Environmental and Energy Engineering, 15–16 February, Chennai, India, 2018.

and electrochemical methods can lead to the formation of toxic sludge, which can further complicate the water treatment procedure [5–7]. Hence there is a need for an efficient and environmentally benign method for proper treatment of these pollutants. Recent studies suggest adsorption as an efficient technique in removing heavy metal ions from aqueous solutions. Further it is considered as one of the most eco-friendly and economical treatment. Various materials that are reported as good adsorbents for the removal of Ni(II) ions include zeolites, agro wastes, industrial byproducts, biomass, polymeric materials, etc. [8–11].

Further, incorporating the properties of nanomaterials onto the adsorbents can enhance their efficiency, due to higher surface area to volume ratio. Moreover, nanomaterials are also known for increasing the chemical reactivity of the material [12]. This is due to availability of more number of surface atoms of higher energy. These surface atoms can easily interact with the adsorbates such as metal ion or organic groups. Surface functionalization of these nanoparticles can further increase the adsorption efficiency and can also improve the chances for desorption [13–15]. It is seen that the donor groups such as amino and oxygen groups can efficiently bind with the transition metal ions via electrostatic interactions, covalent interactions, ion exchange, etc. [16,17]. Hence amine groups are preferred as best functionalizing groups for nanomaterials.

In particular, Fe_3O_4 nanoparticles are characterized by their highly paramagnetic nature, which is mainly due to their higher magnetic moments [18]. These are also found to have highly dispersive nature, enhanced catalytic activity and improved adsorption efficiency. Additionally, the magnetic nature of this adsorbent makes its separation from the solution easier [19]. Previous studies establish that the addition of neem extract provides stability to the nanoparticles by avoiding chances for particle agglomeration [20]. This can also control the crystal growth and are used for getting better yield of nanoparticles [21,22]. This is because of the functional groups in neem extract such as hydrocarbons, alkaloids, phenolic groups, glycosides, etc. [23].

The present study focused on finding out the efficiency of neem-coated magnetite nanoparticles modified by amino group, in removing the Ni(II) ions from aqueous solution. A chemical modification onto its surface by an organic group is carried out to increase the adsorption efficiency. The adsorbent is being synthesized by co-precipitation method and conditions such as pH, concentration, temperature, dose and contact time are being optimized. Isotherm and kinetic studies are also being conducted to understand the reaction mechanism and kinetics.

2. Methodology

2.1. Synthesis of adsorbent

The tender neem leaves collected from the nearby locality were washed well with distilled water and crushed in a mortar. 5% neem extract solution is prepared by taking 5 g neem leaves in 100 mL of distilled water. To obtain the neem extract, this solution is boiled around 50°C–60°C for 30 min. The solution is then cooled and filtered using Whatman filter paper 42.

Ferrous sulphate heptahydrate ($FeSO_4.7H_2O$) and Ferric chloride hexahydrate ($FeCl_3.6H_2O$) are mixed in 1:2 ratios and the mixture is stirred along with heating at 60°C for 10 min [24]. To the mixture of Fe(III) and Fe(II) solutions, 20 mL of the prepared neem extract is added along with stirring using a magnetic stirrer and heated for 5 min. 20 mL of ethylene diamine solution is then added to the above solution along with stirring, followed by the addition of NH_3 solution. The final solution is stirred for 45 min, followed by cooling. After several cycles of centrifugal separation, the black precipitate was dried in a vacuum oven at 60°C. The material was then crushed into a powdered form for homogeneity and stored in a glass bottle inside a desiccator for further use.

2.2. Characterization studies

The synthesized adsorbent (magnetite nanoparticles) was characterized through scanning electron microscopy (SEM, Carl Zeiss, Sigma version) to understand the surface morphology. X-ray diffraction (XRD, Ultima IV, Rigaku, Japan) analysis was done to find out the crystallite size and crystalline nature of the material. Fourier transform infrared spectroscopy (FTIR, Nicolet IS 10, USA) was used to find out the various functional groups present on the adsorbent surface. Vibrating sample magnetometer (VSM, VSM 7410, Lakeshore, USA) technique was used to understand the magnetic nature of the sample. Further thermo gravimetric analysis (TGA, TG-DSC, Netzsch, Germany) was carried out to estimate the thermal stability of the material.

2.3. Batch adsorption studies

Stock solution of Ni(II) ions (1,000 mg/L) was prepared by dissolving 4.478 g of $NiSO_4.6H_2O$ in 1,000 mL of distilled water. The required sample solutions of concentrations 100–500 mg/L were prepared by a series of dilution from the 1,000 mg/L stock solution. 0.2 g of adsorbent is added into a stoppered glass bottle and 50 mL of sample solution is added into it. The solution is shaken for 90 min in an orbital incubator shaker (SLM-INC-OS-250) at 150 rpm. The resultant solution is separated from the adsorbent by magnetic separation. The solution pH was adjusted using 0.1 M of HCL and 0.1 M of NaOH. The sample solutions of 100 mg/L with various pH (from 1 to 8) were analyzed, with sample volume as 50 mL and dosage of adsorbent as 0.2 g.

To find out the contact time needed for the reaction to attain equilibrium, different sample solutions of 100 mg/L of Ni(II) solution was shaken with 0.2 g adsorbent at specific time intervals (10–120 min). The effect of temperature on the adsorption process was studied by analyzing sample solutions of 100 mg/L and dosage of 0.2 g at different temperatures (from 293 to 323 K). The concentration of Ni(II) in the solution is analyzed through UV–Visible spectrophotometer, (Shimadzu UV-1700 PharmaSpec spectrophotometer). The Ni(II) solution is added with bromine water, ammonia solution and dimethyl glyoxime solution (1% solution prepared by mixing 1 g in 100 mL methanol) to form a complex. The wavelength of absorbance was fixed at about 445 nm. The adsorption capacity and efficiency can be calculated using Eqs. (1) and (2), respectively [25]:

$$q_e = \frac{\left(C_i - C_f\right) \times V}{m} \tag{1}$$

$$\%\text{efficiency} = \frac{C_i - C_f}{C_i} \times 100 \tag{2}$$

where q_e is the adsorption capacity given in mg/g, C_i and C_f are the initial and final concentrations of the solution, expressed in mg/L, V is the volume in L and m is the adsorbent dosage in g.

Isotherm studies of the adsorbent were carried out by plotting the Langmuir, Freundlich and Dubinin–Radushkevich adsorption isotherms. This can suggest whether adsorption occurs on homogeneous or heterogeneous surfaces. It also helps us to figure out the possibilities of physisorption and chemisorption mechanisms in the present study. In order to find out the reaction pathway and the possible interactions between metal ions and nanoparticles, pseudo-first order and pseudo-second order models were plotted and analyzed. The thermodynamic studies were conducted in order to confirm the endothermic or exothermic nature of the adsorption process.

2.4. Desorption studies

Desorption efficiency of the adsorbent was analyzed by using HCl and water as the eluting agents. The strength of the HCl used for the study varied from 0.2 to 0.8 N. 0.2 g of adsorbent was shaken with a 200 mg/L solution and the adsorbent collected after shaking was subjected to three cycles of desorption analysis. All the batch experimental parameters were kept as constant. Desorption efficiency corresponding to both the solutions were analyzed via UV method.

3. Results and discussions

3.1. Characterization of adsorbent

The XRD analysis of the adsorbent is shown in Fig. 1. The six characteristic peaks of Fe_3O_4 at 2θ values of 29.46°, 35.10°, 43.3°, 56.64°, 62.5° and 74.54° are observed. Based on the above values, the particles can be identified as magnetite nanoparticles. In general, sharp peaks indicate the crystalline nature of the material. However, the synthesized sample exhibited some variation in the sharp nature of peaks. This is due to the composite nature of the synthesized material involving the presence of amine and neem functional groups in the nanomaterials. Using the Debye–Scherrer formula given in Eq. (3), the average crystallite size is found to be 29.2 nm [26].

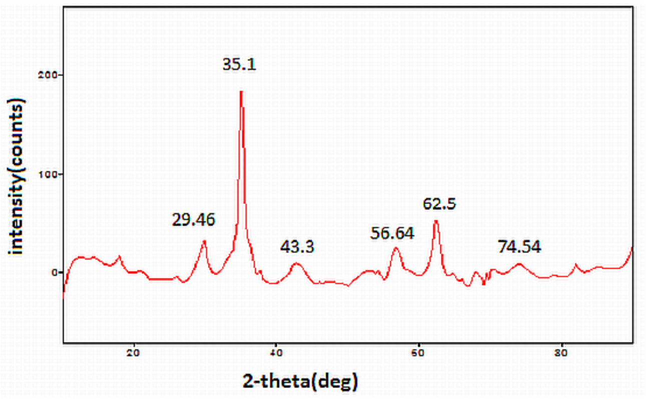

Fig. 1. XRD pattern of the modified Fe_3O_4 nanoparticles.

$$d = \frac{0.9\lambda}{\beta\cos\theta} \tag{3}$$

where d refers to the crystallite size, λ is the X-ray wavelength, θ refers to the Bragg's angle and β implies the full width at half maximum value of XRD lines.

The FTIR spectra of the adsorbent, analyzed within the range of 4,000–500 cm^{-1}, are shown in Fig. 2. A small stretching with two bands at around 3,646 cm^{-1} is due to the N–H stretching of primary amines. This indicates the successful functionalization of amine groups onto nanoparticles surfaces. A very broad peak from 3,500 to 3,000 cm^{-1} is due to an O–H stretching and a peak at 1,633 cm^{-1} represents the carbonyl bond stretching in an amide group. Less intense peak near 1,111 cm^{-1} indicates the presence of alcoholic C–O (R–OH) stretching. The carbonyl stretching representing the amide bonds confirms the neem extract coating onto the material. A sharp peak near to 571 cm^{-1} confirms the formation of Fe_3O_4 nanoparticles [27,28].

To understand the magnetic nature of the amine-modified adsorbent, VSM analysis is carried out. The result of the analysis conducted at room temperature is shown in Fig. 3. The typical s-shaped thin curve and the absence of hysteresis show that the particle is superparamagnetic in nature [26]. Further the remnant magnetization value is also found to be less. A magnetic nanoparticle will usually have a value of 92 emu/g [29]. The saturation magnetization value of the amine-modified nanoparticles was found to be 38.5 emu/g. A similar decreased value is observed in the other studies of Fe_3O_4 nanoparticles [30]. However, a low value reported in the amine-modified nanoparticles was due to the amine and neem matrix of the iron oxide nanoparticles. Nevertheless this value is sufficient to separate the magnetic nanoparticles from the aqueous system after the adsorption process.

Surface topography of the material and texture was analyzed using SEM technique. The different resolutions of SEM images of the amine-modified nanoparticles display the cubical shaped particles as shown in Fig. 4. Due to the role of neem extract and amine-based functional groups, no prominent clusters or agglomerations are noticed in the images. Apart from imparting necessary functional groups on the adsorbent, both the neem and the amine groups helped in capping the nanoparticles. Further, the results of the Energy dispersive X-ray spectroscopy (EDX) analysis are shown in Fig. 5. The EDX images reveal the occurrence of carbon groups which is an indication of the organic coating of the sample. The iron is an indication for magnetite nanoparticles and nitrogen emerged from the amine group. In the EDX analysis of the nanoparticles after adsorption, a peak is shown for nickel, and this confirms the nickel adsorption onto the modified nanoparticles.

TGA of the adsorbent explains about the thermal stability of the adsorbent. The heating rate was taken as 10°C/min and the temperature was raised up to 1,400°C. In Fig. 6, the initial mass change up to about 200°C is due to the decomposition of water molecules. Further loss of mass up to 400°C is due to the decomposition of the organic moieties present on the

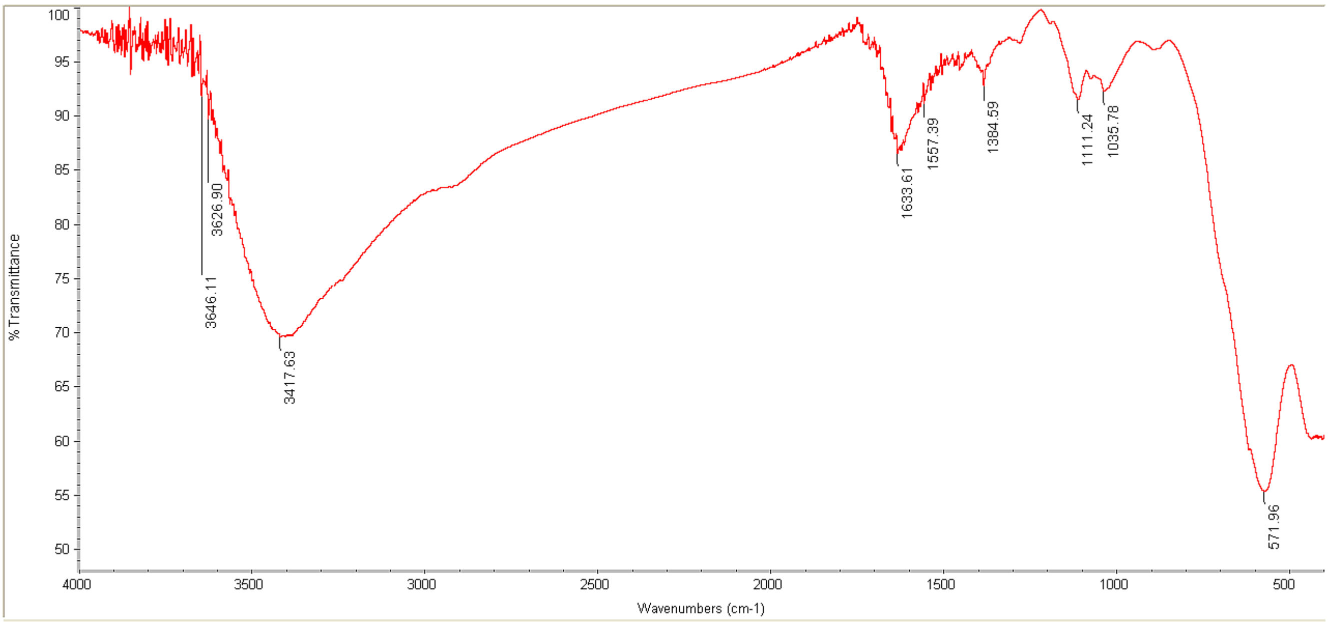

Fig. 2. FTIR spectra of modified Fe_3O_4 nanoparticles.

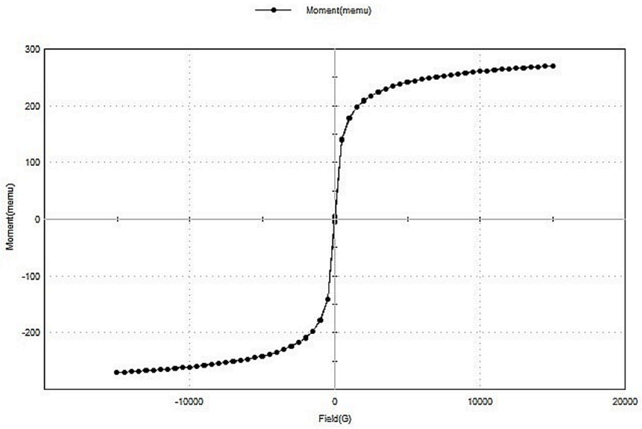

Fig. 3. VSM analysis of modified Fe_3O_4 nanoparticles.

surface of adsorbent. From 400°C to 1,200°C, a flat curve is observed and this indicates that the material is stable up to about 1,200°C [31,32]. Another remarkable mass loss of about 3% has occurred near to 1,289°C. A final mass loss of around 15% corresponds to the organic groups bounded onto the nanoparticles surfaces.

3.2. Results of batch studies

3.2.1. Effect of concentration

Adsorption of Ni(II) by the modified magnetite nanoparticles was largely influenced by the concentration of Ni(II) solution. By fixing the adsorbent dosage as 0.2 g, pH of Ni(II) solution as 6 and the contact time as 90 min, the concentration of Ni(II) solution was varied from 100 to 500 mg/L, at room temperature. From Fig. 7, it can be inferred that as concentration increased from 100 to 500 mg/L, efficiency of adsorption decreased from 51.05% to 5.8%. The reason behind such a decreased efficiency with respect to higher concentrations is that, the number of available adsorption sites for a specific amount of adsorbent is fixed [33]. The reverse trend is observed when uptake capacity is plotted against concentration. The uptake capacity corresponding to 100 mg/L is 12.76 mg/g and that for 500 mg/L is 19.75 mg/g (figure not shown).

3.2.2. Effect of pH

The effect of pH of the Ni(II) solution on the efficiency of adsorption was studied by varying the solution pH from 1 to 8 at a fixed concentration of 100 mg/L, dosage of 0.2 g and contact time as 90 min at room temperature. The graph is given in Fig. 8. The studies point out that the maximum efficiency is at a pH of 6. At higher pH due to electrostatic attraction between nickel ions and negatively charged binding sites the adsorption increases [34]. But at lower pH, the Ni(II) ions and protons tend to occupy the adsorption sites due to enriched H^+ ions developing a repulsive action with cationic Ni(II) ions and decreases the efficiency of adsorption [35]. Further when the pH is increased beyond 6, the efficiency is gradually decreasing due to the formation of hydroxides of nickel which hinders the adsorption process [36].

3.2.3. Effect of contact time

The change in the efficiency of adsorption with contact time has been analyzed. For a fixed concentration of 100 mg/L at pH of 6 and dosage of 0.2 g at room temperature, the contact time was varied from 10 to 120 min. As per the results given in Fig. 9, the adsorption efficiency is gradually increasing with increase in contact time and then reaches a saturation limit, which implies that there is a decrease in the availability of adsorption sites [37,38]. The efficiency of adsorption is found to be 50.86% at 90 min. Most of the active sites on the adsorbent surface are covered by the metal ions and this reaches equilibrium at around 90 min.

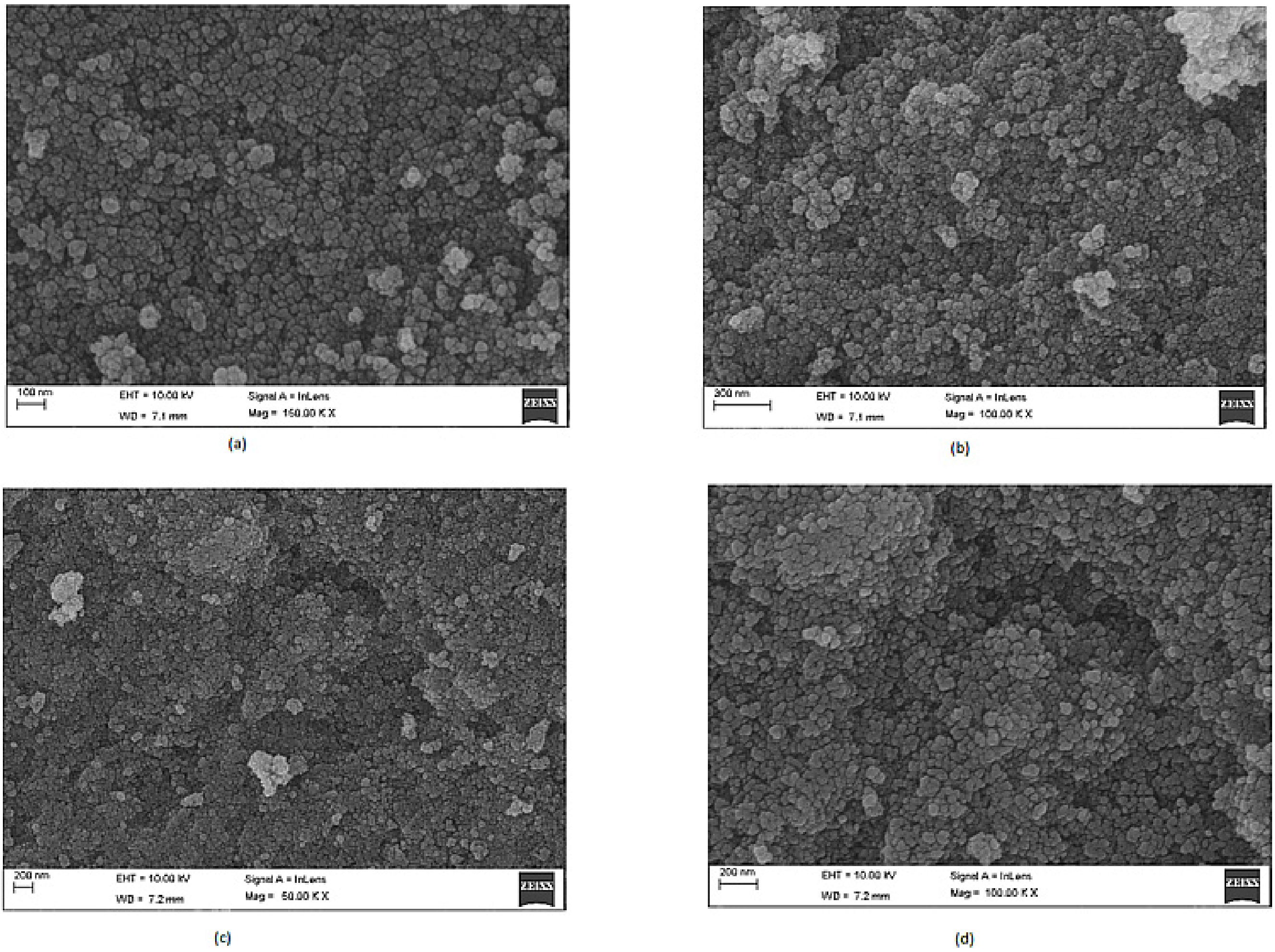

(a) (b) (c) (d)

Fig. 4. SEM images of modified Fe_3O_4 nanoparticles.

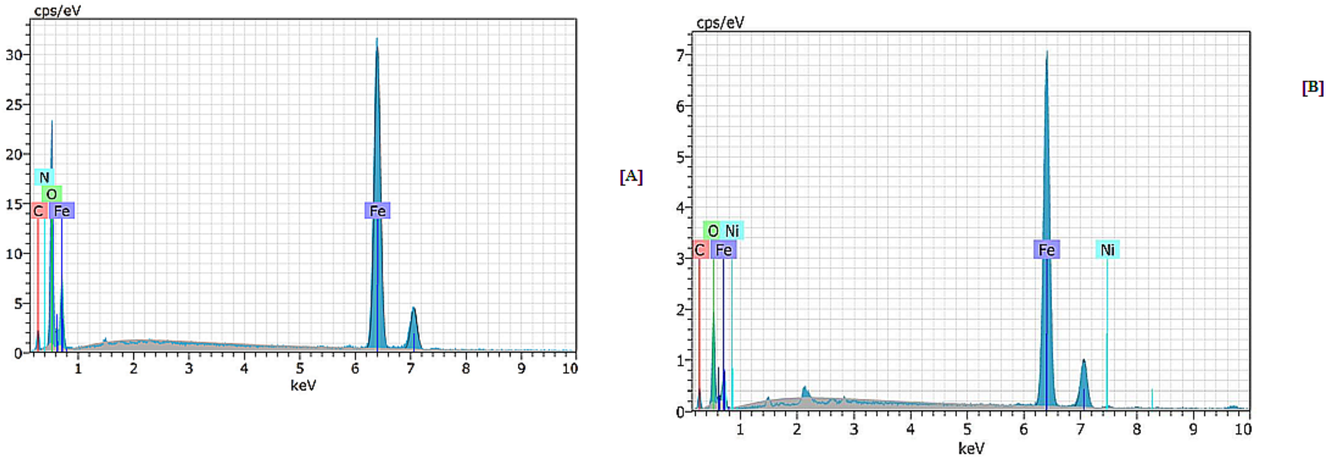

Fig. 5. EDX analysis of modified Fe_3O_4nanoparticles before and after adsorption.

3.2.4. *Effect of dosage*

As per the graph shown in Fig. 10, the adsorption efficiency is found to be increasing with an increase in the amount of adsorbent being used. After reaching a saturation limit, increase in dosage causes decrease in adsorption efficiency. Initial increase of adsorption efficiency is due to availability of more surface area. But with very higher dosage there can be particle aggregation. There will be a higher number of active sites for adsorption but the metal ions to be adsorbed will be less in number [39]. The uptake capacity corresponding to 0.2 g adsorbent is 12.96 mg/g while that for

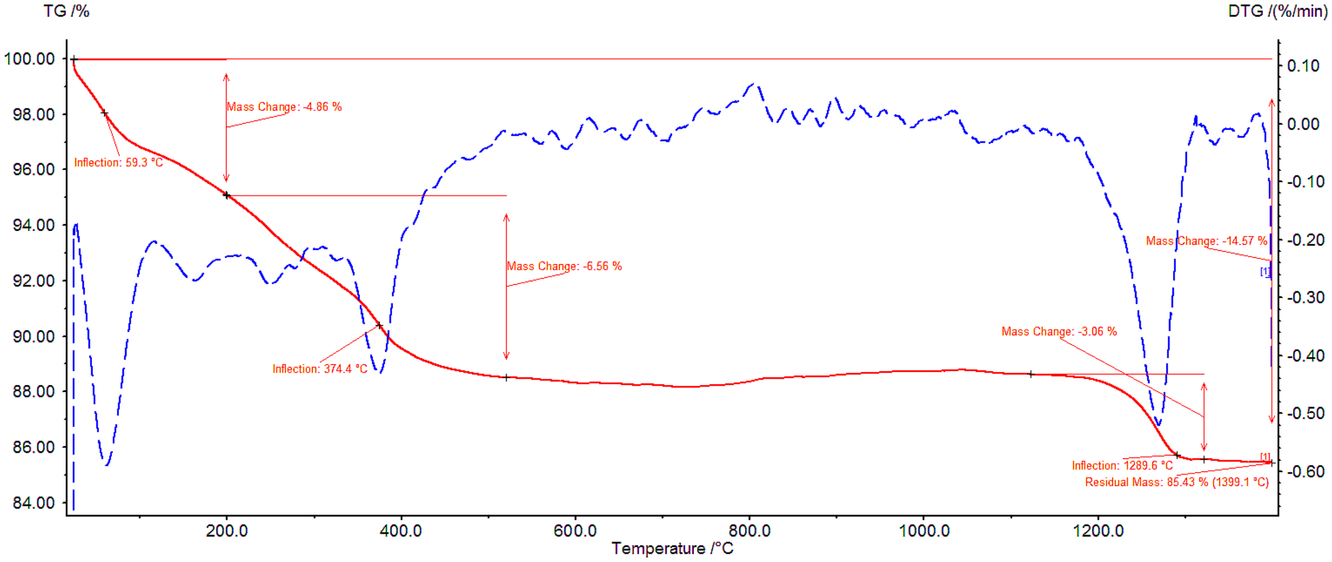

Fig. 6. TGA of modified Fe_3O_4 nanoparticles.

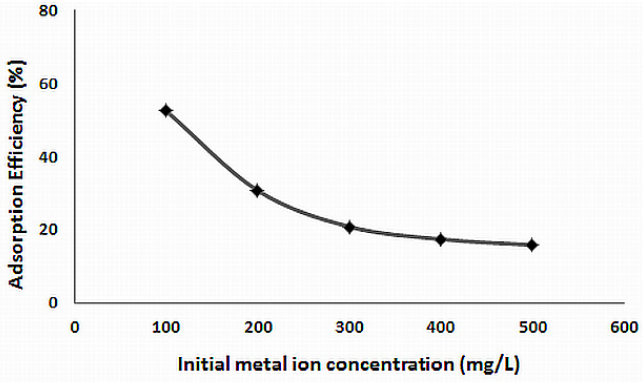

Fig. 7. Effect of initial metal ion concentration on the adsorption efficiency.

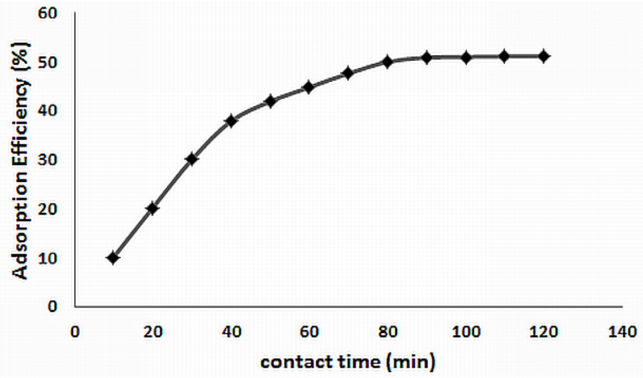

Fig. 9. Effect of contact time on the adsorption efficiency.

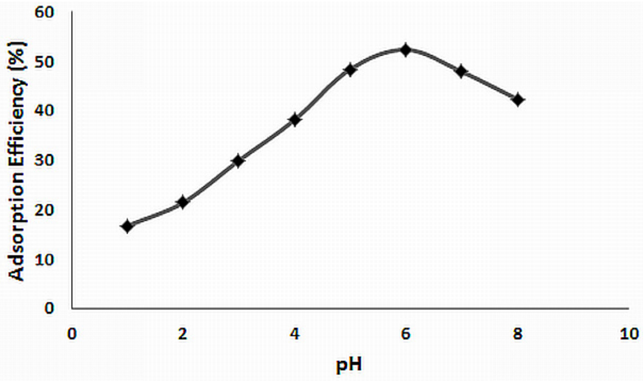

Fig. 8. Effect of pH on the adsorption efficiency.

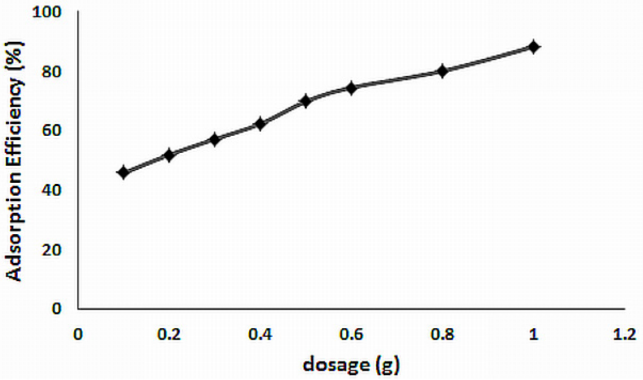

Fig. 10. Effect of adsorbent dose on the adsorption efficiency.

a 1 g adsorbent is 2.8 mg/g. This trend can be explained on the basis of relating the uptake capacity and dosage. We can find that as dosage (m) is less, the adsorption capacity (q_e) is more according to Eq. (1). Hence 0.2 g is being fixed as the adsorbent dosage for carrying out further experiments.

3.2.5. Effect of temperature

The effect of temperature on the adsorption efficiency is studied. The analysis is conducted by varying temperature from 298 to 338 K, at fixed concentration of 100 mg/L, pH as 6, dosage as 0.2 g and time as 90 min. Variation of adsorption efficiency with increase in temperature is shown in Fig. 11. Adsorption efficiency is found to be decreasing from 298 to 338 K. This can be attributed to the fact that increase in temperature can cause a damage to the binding sites or can lead to desorption of metal ions from adsorbent surface [40,41]. Hence, the reaction tends to be exothermic in nature.

3.3. Isotherm studies

Langmuir, Freundlich and Dubinin–Radushkevich isotherm models were used for studying the equilibrium of adsorption process. The Langmuir isotherm model fits more for adsorption on a homogeneous surface implying that the adsorbent surface contains finite number of identical active sites [42]. In Langmuir model, the interaction between the adsorbed species is considered to be absent. The equation for adsorption capacity with respect to Langmuir isotherm model is given in Eq. (4).

$$\frac{1}{q_e} = \frac{1}{q_m} + \frac{1}{q_m K_L C_e} \tag{4}$$

where q_m is the maximum uptake of metal ions corresponding to the saturation of adsorption sites given in mg/g, C_e is the final concentration in mg/L, K_L is the Langmuir constant. R_L is the separation factor or the affinity between adsorbate and adsorbent [35]. R_L is expressed mathematically as per Eq. (5).

$$R_L = \frac{1}{1 + K_L C_O} \tag{5}$$

C_o is the initial concentration in mg/L. If the value of $R_L = 0$, the reaction is irreversible. If $R_L = 1$, the reaction is linear. $R_L > 1$ implies an unfavorable reaction and $0 < R_L < 1$ implies a favorable reaction [43].

The Freundlich model is studied using Eq. (6) [44]:

$$\log q_e = \log K_f + \frac{1}{n} \log C_e \tag{6}$$

K_f and n are Freundlich constants related to adsorption capacity and adsorption intensity, respectively. C_e is the equilibrium concentration of adsorbate given in mg/L. In the Freundlich model, the adsorbent surface is considered to be a heterogeneous one [45].

The results of Langmuir and Freundlich model analysis is shown in Table 1. From the data obtained after plotting Langmuir and Freundlich isotherms (Figs. 12 and 13) it can be understood that the adsorption process is more fitting toward Freundlich isotherm. This is indicated by a higher coefficient of determination, $R^2 = 0.908$. This indicates that the adsorption occurs on a heterogeneous surface and both physisorption as well as chemisorption are likely to occur in the present study. The values of separation factor R_L obtained from the Langmuir plot falls between 0 and 1. This suggests that the adsorption process is favorable. The R_L value corresponding to each of the concentrations is given in Table 2. Based on the investigations on Freundlich model, a better adsorption and stronger bond between the adsorbate and adsorbent is marked by a lower $1/n$ value. An efficient

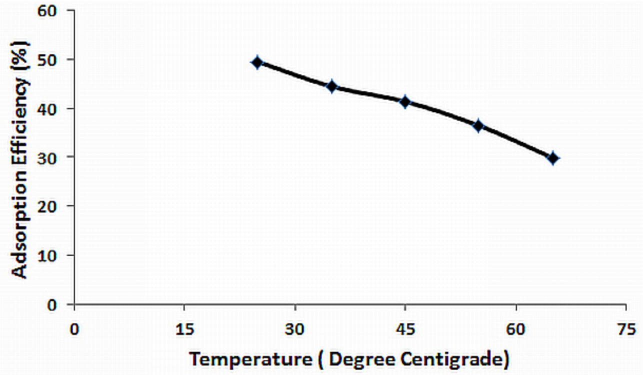

Fig. 11. Effect of temperature on the adsorption efficiency.

Table 1
Results of the Langmuir and Freundlich isotherm analysis

Langmuir model	Freundlich model
$R^2 = 0.837$	$R^2 = 0.908$
$K_L = 0.0395$ L/mg	$K_f = 6.237$ mg$^{1-(1/n)}$ L$^{1/n}$ g^{-1}
$q_m = 19.23$ mg/g	$1/n = 0.180$
$R_L = 0.202$ to 0.031	$n = 5.55$
(from 100 to 500 mg/L)	

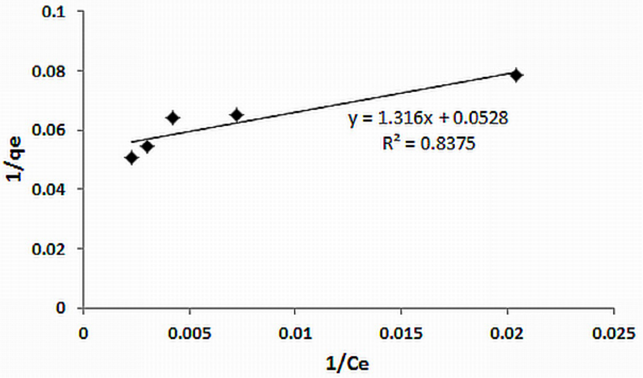

Fig. 12. Langmuir isotherm plot for nickel adsorption.

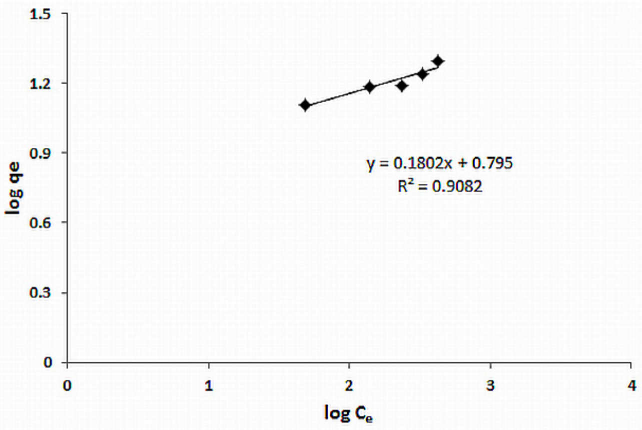

Fig. 13. Freundlich isotherm plot for nickel adsorption.

adsorbent is characterized by a 1/*n* value between 0.2 and 0.8. An experimental 1/*n* value of 0.180 obtained in the present study implies that the adsorption is favorable [46]. The maximum amount of metal ions being adsorbed corresponding to the saturation of adsorption sites (q_m) is found to be 19.23 mg/g. The adsorption capacities of the various other iron oxide based adsorbents are compared and listed in Table 3.

The Dubinin–Radushkevich isotherm explains about the mean free energy of the adsorption (*E*) per molecule of the adsorbate [52]. The equations governing this isothermal model are as follows [53]:

$$q_e = q_m e^{-B\epsilon^2} \tag{7}$$

$$\ln q_e = \ln q_m - B\epsilon^2 \tag{8}$$

$$\epsilon^2 = RT\ln(1 + \frac{1}{C_e}) \tag{9}$$

Table 2
Values of R_L corresponding to different concentrations

Concentration (mg/L)	R_L
100	0.2020
200	0.1123
300	0.077
400	0.059
500	0.0310

Table 3
Comparative study of the adsorption capacity of various iron oxide adsorbents

Adsorbents	Adsorption capacity (mg/g)	References
Fe_3O_4-tea waste	38.30	[35]
Iron oxide-coated sewage sludge	7.8	[39]
Fe_3O_4	35.6	[45]
Natural iron oxide coated sand	1	[47]
Multi-walled carbon nano tube/iron oxide magnetic composite	9.18	[48]
Iron oxide-coated waste silica	4.25	[49]
Magnetic Fe @ graphite nano-composite	9.2	[50]
Nanoscale zero-valent iron-impregnated cashew nut shell	70.05	[51]
Green synthesized amine-modified Fe_3O_4 nanoparticles	19.23	Present study

From the graph plotted against ε^2 and ln q_e (Fig. 14), the values corresponding to q_m (maximum adsorption capacity in mg/g) and *B* (Dubinin–Radushkevich constant in mol^2/J^2) were found out. The value of *E* (expressed in kJ/mol) was calculated as follows [54]:

$$E = \frac{1}{\sqrt{2B}} \tag{10}$$

Based on the value obtained for *E*, the type of adsorption process can be determined. For an *E* value less than 8 kJ/mol, physisorption is favored. If 8 kJ/mol < *E* < 16 kJ/mol, the adsorption occurs due to exchange of ions. For an *E* value greater than 16 kJ/mol, chemisorption is dominating [55].

From the results obtained after analyzing the Dubinin–Radushkevich model, the maximum adsorption capacity, q_m and the constant, *B* is estimated as 17.2 mg/g and 0.0001 mol^2/J^2, respectively. The value of *E* is calculated to be 0.0701 kJ/mol. Even though the value of *E* falls under the range for physisorption, a very low R^2 value (0.67) suggests that this model does not give a best fit.

3.4. Kinetic studies

The rate constant for the reaction and the mechanism of adsorption process was determined by studying the adsorption kinetics. The mechanism of an adsorption process does depend upon the parameters such as adsorbent structure, nature of the sorbate and sorbent, etc. [56]. The expressions for finding out the first and second order kinetics are given in Eqs. (11) and (12), respectively [57]:

$$\log\left(q_e - q_t\right) = \log q_e - \frac{k_1}{2.303}t \tag{11}$$

$$\frac{t}{q_t} = \frac{1}{q_e}t + \frac{1}{h} \tag{12}$$

where $h = k_2 q_e^2$.

Here q_e (mg/g) represents the amount of nickel ions being adsorbed at equilibrium while q_t (mg/g) refers to the amount of nickel ions adsorbed at time *t*. k_1 and k_2 in the equation represents the rate constant corresponding to the pseudo-first and pseudo-second order reactions, respectively.

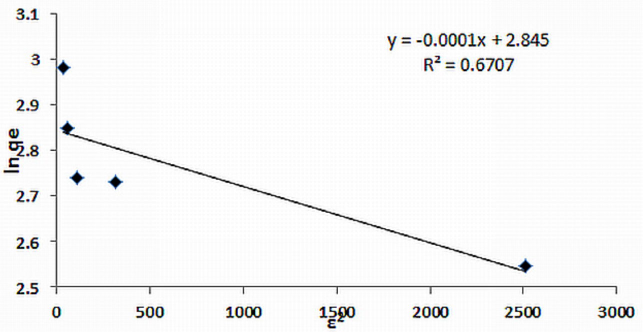

Fig. 14. Dubinin–Radushkevich isotherm plot.

The graphs corresponding to the pseudo-first order and pseudo-second order model for a 100 mg/L of nickel solution is given in Figs. 15 and 16. A comparison of the results of two types of kinetic studies is given in Table 4. On the basis of R^2 value, the reaction fits more toward pseudo-second order model and the calculated q_e values are comparable with the experimental q_e value (13.14 mg/g). Hence, the kinetic studies suggest that the reaction preferably follows pseudo-second order kinetics and the favored adsorption type is determined to be chemisorption [55,58].

3.5. Thermodynamic studies

In order to find out the nature of the adsorption process, thermodynamic studies were conducted. For any reaction, the spontaneity and degree of randomness are marked by the change in free energy (ΔG^0) and entropy change (ΔS^0), respectively. Further the change in enthalpy (ΔH^0) explains whether the reaction is exothermic or endothermic in nature. These thermodynamic factors were calculated on the basis of the following equations [59,60]:

$$K_c = \frac{C_a}{C_e} \tag{13}$$

$$\Delta G^0 = -RT\ln K_c \tag{14}$$

$$\Delta G^{^0} = \Delta H^0 - T\Delta S^0 \tag{15}$$

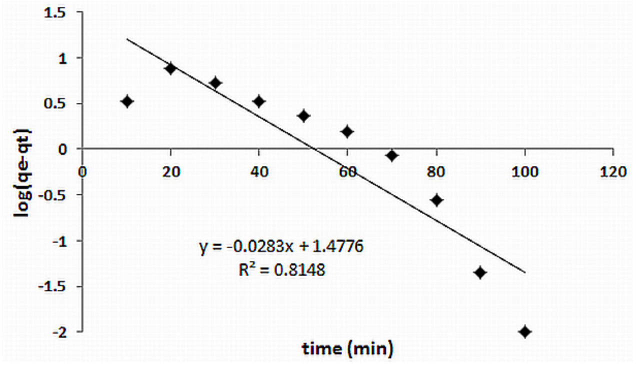

Fig. 15. Pseudo-first order model plot for nickel adsorption.

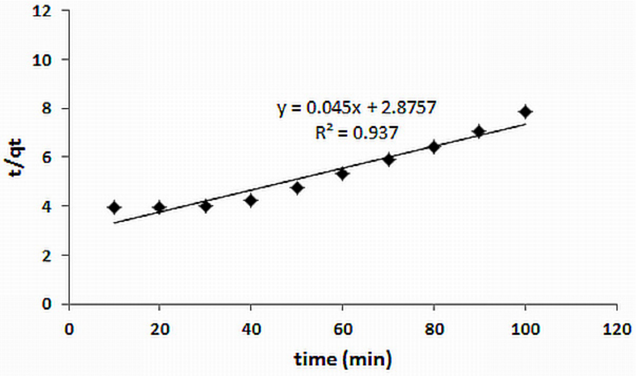

Fig. 16. Pseudo-second order model plot for nickel adsorption.

$$\ln K_c = \frac{\Delta S^0}{R} - \frac{\Delta H^0}{RT} \tag{16}$$

K_c refers to the distribution coefficient of adsorption. C_a and C_e indicate the concentration of the Ni(II) ions on the adsorbent and in the solution, respectively. Both the terms are expressed in mg/L. T implies the absolute temperature (given in K) and R refers to the universal gas constant, 8.314 J/mol/K.

The experiment was carried out at temperatures ranging from 298 to 338 K for a 100 mg/L solution at a pH of 6, using a 0.5 g adsorbent. The values of ΔG^0, ΔS^0 and ΔH^0 obtained from the thermodynamic studies have been shown in Table 5. The negative value of ΔG^0 suggests the reaction to be spontaneous in nature. The values of ΔS^0 and ΔH^0 were obtained from the graph plotted between ln K_c and 1/T (Fig. 17). The negative value of ΔH^0 points out the exothermic nature of adsorption process [61,62]. A similar type of result is obtained in the case of cadmium adsorption using modified *Caryota urens* seeds [63]. The negative value of ΔS^0 says that the degree of randomness of the reaction has decreased [64].

3.6. Desorption studies

The efficiency of desorption was determined by eluting the adsorbent with water and HCl. No specific desorption

Table 4
Results of kinetic studies based on pseudo-first order and pseudo-second order model

Pseudo-first order model	Pseudo-second order model
$R^2 = 0.814$	$R^2 = 0.937$
$k_1 = 0.0644$ min^{-1}	$k_2 = 7.04 \times 10^{-4}$ g/mg/min
q_e (experimental) = 13.13 mg/g	q_e (experimental) = 13.13 mg/g
q_e (calculated) = 29.99 mg/g	q_e (calculated) = 22.22 mg/g

Table 5
Results obtained from thermodynamic studies

ΔH^0 (kJ/mol)	ΔS^0 (kJ/mol/K)	ΔG^0 (kJ/mol)				
–17.02	0.05	298 K	308 K	318 K	328 K	338 K
		–2.07	–1.56	–0.96	–0.51	–0.05

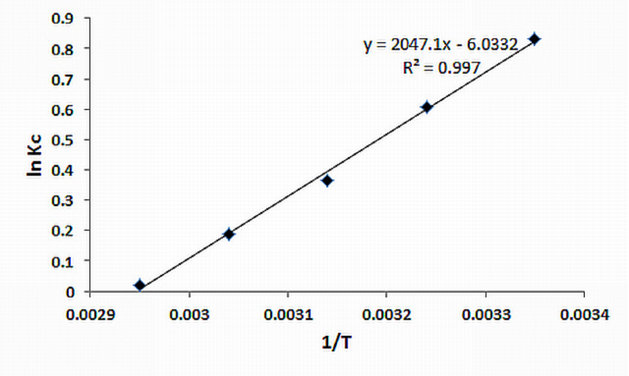

Fig. 17. Thermodynamic studies for nickel adsorption.

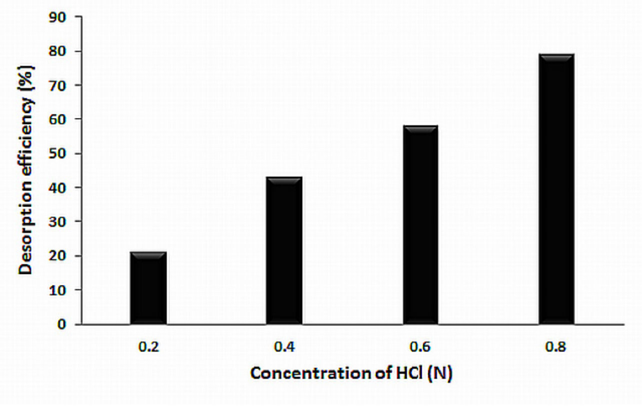

Fig. 18. Desorption study using HCl for nickel adsorption.

was reported on using water as the eluting agent. This shows that no chances for physical adsorption are prevalent in the present study. But when the adsorbent was treated with HCl (0.2–0.8 N) there was a remarkable increase in the desorption efficiency (Fig. 18). With increase in the acid concentration a similar observation was reported for Ni(II) adsorption on using maghemite nanoparticles [65]. The maximum desorption efficiency with respect to 0.8 N HCl was found to be 79%. The positive results obtained using this acid-based reactive eluting agent expresses the likelihood of chemical adsorption in the current study. However, after successive cycles of desorption analysis, roughly 20% reduction in desorption efficiency is noticed (figure not shown). Further increase in the concentration of acid can lead to the damage of adsorbent material and hence not carried out. The present desorption analysis is carried out using HCl due its higher acidic nature than any other acid-based eluting agents.

4. Conclusions

The present study has mainly focused on finding out the efficiency of the amine-modified green synthesized Fe_3O_4 nanoparticles for the adsorption of Ni(II) ions from aqueous solution. The material was synthesized via co-precipitation method and was characterized using techniques such as FTIR, XRD, SEM, EDX, TGA and VSM. The adsorption parameters such as concentration, pH, dosage, contact time and temperature were optimized. The reaction was found to be exothermic in nature. The isotherm studies using Langmuir and Freundlich adsorption isotherms suggest that the process is likely to be a combination of both physisorption as well as chemisorption. The Langmuir adsorption capacity of the material is estimated to be 19.23 mg/g. Further the kinetic studies showed that the process follows pseudo-second order kinetics suggesting chemisorption. Based on the obtained results, the possible interaction between the Ni(II) ions and the adsorbent is suggested as electrostatic and covalent interactions. The thermodynamic studies reveal the exothermic nature of adsorption. Further an improved desorption efficiency of 79% is reported in the current study. Hence the present adsorption system using green synthesized amine-modified nano-based adsorbent is proposed to be an effective alternate for the removal of nickel ions from aqueous solution.

Acknowledgment

The authors hereby would like to express their sincere gratitude to the sophisticated analytical instrument facility (SAIF) of IIT, Madras, and for the services rendered in analyses such as VSM and TGA-DTG.

References

[1] M.A. Barakat, New trends in removing heavy metals from industrial wastewater, Arabian J. Chem., 4 (2011) 361–377.
[2] G.C. Panda, S.K. Das, T.S. Bandopadhyay, A.K. Guha, Adsorption of nickel on husk of *Lathyrus sativus:* behavior and binding mechanism, Colloids Surf., B, 57 (2007) 135–142.
[3] C.F. Carolin, P.S. Kumar, A. Saravanan, G.J. Joshiba Mu. Noushad, Efficient techniques for the removal of toxic heavy metals from aquatic environment: a review, J. Environ. Chem. Eng., 5 (2017) 2782–2799.
[4] S. Suganya, K. Kayalvizhi, P.S. Kumar, A. Saravanan, V.V. Kumar, Biosorption of Pb(II), Ni(II) and Cr(VI) ions from aqueous solution using *Rhizoclonium tortuosum*: extended application to nickel plating industrial wastewater, Desal. Wat. Treat., 57 (2016) 25114–25139.
[5] N. Akhtar, J. Iqbal, M. Iqbal, Removal and recovery of nickel (II) from aqueous solution by loofa sponge-immobilized biomass of *Chlorella sorokiniana*: characterization studies, J. Hazard. Mater., 8 (2004) 85–94.
[6] P.S. Kumar, R. Sivaranjanee, P. Sunder Rajan, A. Saravanan, Carbon sphere: synthesis, characterization and elimination of toxic Cr(VI) ions from aquatic system, J. Ind. Eng. Chem., 60 (2018) 307–320.
[7] A. Saravanan, P.S. Kumar, B. Preetha, Optimization of process parameters for the removal of chromium(VI) and nickel(II) from aqueous solutions by mixed biosorbents (custard apple seeds and *Aspergillus niger*) using response surface methodology, Desal. Wat. Treat., 57 (2016) 14530–14543.
[8] V.K. Gupta, C.K. Jain, I. Ali, M. Sharma, V.K. Saini, Removal of cadmium and nickel from wastewater using bagasse fly ash—a sugar industry waste, Water Res., 37 (2003) 4038–4044.
[9] S.S. Shukla, L.J. Yu, K.L. Dorris, A. Shukla, Removal of nickel from aqueous solutions by sawdust, J. Hazard. Mater., 121 (2005) 243–246.
[10] N. Ahalya, T.V. Ramachandra, R.D. Kanamadi, Biosorption of heavy metals, Res. J. Chem. Environ., 7 (2003) 71–79.
[11] A. Saravanan, P.S. Kumar, P. Sunder Rajan, A.S. Narayan, A. Dutta, Influence of ultrasonication on preparation of novel material for heavy metal removal from water/wastewater, Korean J. Chem. Eng., 33 (2016) 2716–2731.
[12] Y.C. Sharma, V. Srivastava, V.K. Singh, S.N. Kaul, C.H. Weng, Nano-adsorbents for the removal of metallic pollutants from water and wastewater, Environ. Technol., 30 (2009) 583–609.
[13] M. Khajeh, S. Laurent, K. Dastafkan, Nanoadsorbents: classification, preparation, and applications (with emphasis on aqueous media), Chem. Rev., 113 (2013) 7728–7768.
[14] P.Z. Ray, H.J. Shipley, Inorganic nano-adsorbents for the removal of heavy metals and arsenic: a review, RSC Adv., 5 (2015) 29885–29907.
[15] S. Suganya, P.S. Kumar, Influence of ultrasonic waves on preparation of active carbon from coffee waste for the reclamation of effluents containing Cr(VI) ions, J. Ind. Eng. Chem., 60 (2018) 418–430.
[16] Y.G. Zhao, H.Y. Shen, S.D. Pan, M.Q. Hu, Q.H. Xia, Preparation and characterization of amino-functionalized nano-Fe_3O_4 magnetic polymer adsorbents for removal of chromium (VI) ions, J. Mater. Sci., 45 (2010) 5291–5301.
[17] S.H. Huang, D.H. Chen, Rapid removal of heavy metal cations and anions from aqueous solutions by an amino-functionalized magnetic nano-adsorbent, J. Hazard. Mater., 163 (2009) 174–179.
[18] M. Takafuji, S. Ide, H. Ihara, Z. Xu, Preparation of poly (1-vinylimidazole)-grafted magnetic nanoparticles and their application for removal of metal ions, Chem. Mater., 16 (2004) 1977–1983.

[19] T.V. Novi, V.V. Kumar, P.S. Kumar, C. Christy, S.S. Lavanyaa, D. Vishnu, A. Saravanan, V.V. Kumar, S. Sivanesan, Review on nanoadsorbents: a solution for heavy metal removal from wastewater, IET Nanobiotechnol., 11 (2017) 213–224.

[20] W.M. Daoush, Co-precipitation and magnetic properties of magnetite nanoparticles for potential biomedical applications, J. Nanomed. Res., 5 (2017) 00118.

[21] M. Pattanayak, P.L. Nayak, Green synthesis and characterization of zero valent iron nanoparticles from the leaf extract of *Azadirachta indica* (Neem), World J. Nano Sci. Technol., 2 (2013) 6–9.

[22] S. Ahmed, M. Ahmed, B.L. Swami, S. Ikram, A review on plants extract mediated synthesis of silver nanoparticles for antimicrobial applications: a green expertise, J. Adv. Res., 7 (2016) 17–28.

[23] Z. Khan, J.I. Hussain, A.A. Hashmi, Shape-directing role of cetyltrimethylammonium bromide in the green synthesis of Ag-nanoparticles using Neem (*Azadirachta indica*) leaf extract, Colloids Surf., B, 95 (2012) 229–234.

[24] Z.L. Liu, Y.J. Liu, K.L. Yao, Z.H. Ding, J. Tao, X. Wang, Synthesis and magnetic properties of Fe_3O_4 nanoparticles, J. Mater. Synth. Process., 10 (2002) 83–87.

[25] E. Gunasundari, P.S. Kumar, Adsorption isotherm, kinetics and thermodynamic analysis of Cu (II) ions onto the dried algal biomass (*Spirulina platensis)*, J. Ind. Eng. Chem., 56 (2017) 129–144.

[26] H.E. Ghandoor, H.M. Zidan, M.M.H. Khalil, M.I.M. Ismail, Synthesis and some physical properties of magnetite (Fe_3O_4) nanoparticles, Int. J. Electrochem. Sci., 7 (2012) 5734–5745.

[27] Z.L. Liu, X. Wang, Synthesis of magnetite nanoparticles in W/O microemulsion, J. Mater. Sci., 39 (2004) 2633–2636.

[28] K. Nithya, A. Sathish, P.S. Kumar, T. Ramachandran, Fast kinetics and high adsorption capacity of green extract capped superparamagnetic iron oxide nanoparticles for the adsorption of Ni(II) ions, J. Ind. Eng. Chem., 59 (2018) 230–241.

[29] S. Wang, J. Huang, H. Yan, K. Liu, Size-controlled preparation of magnetite nanoparticles in the presence of graft copolymers, J. Mater. Chem., 16 (2006) 298–303.

[30] Y.H. Zheng, Y. Cheng, F. Bao, Y.S. Wang, Synthesis and magnetic properties of Fe_3O_4 nanoparticles, Mater. Res. Bull., 41 (2006) 525–529.

[31] D. Maity, S.G. Choo, J. Yi, J. Ding, J.M. Xue, Synthesis of magnetite nanoparticles via a solvent-free thermal decomposition route, J. Magn. Magn. Mater., 321 (2009) 1256–1259.

[32] M. Bhaumik, K. Setshedi, A. Maityand, M.S. Onyango, Chromium (VI) removal from water using fixed bed column of polypyrrole/Fe_3O_4 nanocomposite, Sep. Purif. Technol., 110 (2013) 11–19.

[33] P.S. Kumar, A.S.L. Sai Deepthi, R. Bharani, C. Prabhakaran, Adsorption of Cu(II), Cd(II) and Ni(II) ions from aqueous solution by unmodified *Strychnos potatorum* seeds, Eur. J. Environ. Civil Eng., 17 (2013) 293–314.

[34] K. Nithya, A. Sathish, P.S. Kumar, T. Ramachandran, An insight into the prediction of biosorption mechanism, and isotherm, kinetic and thermodynamic studies for Ni(II) ions removal from aqueous solution using acid treated biosorbent: the *Lantana camara* fruit, Desal. Wat. Treat., 80 (2017) 276–287.

[35] P. Panneerselvam, N. Morad, K.A. Tan, Magnetic nanoparticle (Fe_3O_4) impregnated onto tea waste for the removal of nickel (II) from aqueous solution, J. Hazard. Mater., 186 (2011) 160–168.

[36] P.S. Kumar, K. Ramakrishnan, R. Gayathri, Removal of Nickel(II) from aqueous solutions by Ceralite IR 120 cationic exchange resins, J. Eng. Sci. Technol., 5 (2010) 234–245.

[37] P.S. Kumar, K. Kirthika, Equilibrium and Kinetic study of adsorption of nickel from aqueous solution onto bael tree leaf powder, J. Eng. Sci. Technol., 4 (2009) 396–406.

[38] P.S. Kumar, S. Ramalingam, V. Sathyaselvabala, S.D. Kirupha, V. Sathyaselvabala, Removal of copper(II) ions from aqueous solution by adsorption using cashew nut shell, Desalination, 266 (2011) 63–71.

[39] T. Phuengprasop, J. Sittiwong, F. Unob, Removal of heavy metal ions by iron oxide coated sewage sludge, J. Hazard. Mater., 186 (2011) 502–507.

[40] A. Ozerand, D. Ozer, Comparative study of the biosorption of Pb (II), Ni (II) and Cr (VI) ions onto *S. cerevisiae*: determination of biosorption heats, J. Hazard. Mater., 100 (2003) 219–229.

[41] P.S. Kumar, S. Ramalingam, R.V. Abhinaya, S.D. Kirupha, A. Murugesan, S. Sivanesan, Adsorption of metal ions onto the chemically modified agricultural waste, Clean Water Air Soil, 40 (2012) 188–197.

[42] Z. Aksu, Determination of the equilibrium, kinetic and thermodynamic parameters of the batch biosorption of nickel (II) ions onto *Chlorella vulgaris*, Process Biochem., 38 (2002) 89–99.

[43] P.S. Kumar, R. Gayathri, C. Senthamarai, M. Priyadharshini, P.S.A. Fernando, R. Srinath, V.V. Kumar, Kinetics, mechanism, isotherm and thermodynamic analysis of adsorption of cadmium ions by surface modified *Strychnos potatorum* seeds, Korean J. Chem. Eng., 29 (2017) 1752–1760.

[44] P.S. Kumar, C. Vincent, K. Kirthika, K.S. Kumar, Kinetics and equilibrium studies of Pb^{2+} ions removal from aqueous solutions by use of nano silversol coated activated carbon, Braz. J. Chem. Eng., 27 (2010) 339–346.

[45] S. Mahdavi, M. Jalali, A. Afkhami, Removal of heavy metals from aqueous solutions using Fe_3O_4, ZnO, and CuO nanoparticles, J. Nanopart. Res., 14 (2012) 846.

[46] S.U. Yoon, B. Mahanty, H.M. Ha, C.G. Kim, Phenol adsorption on surface-functionalized iron oxide nanoparticles: modeling of the kinetics, isotherm, and mechanism, J. Nanopart. Res., 18 (2016) 170.

[47] N. Boujelben, J. Bouzid, Z. Elouear, Adsorption of nickel and copper onto natural iron oxide-coated sand from aqueous solutions: study in single and binary systems, J. Hazard. Mater., 163 (2009) 376–382.

[48] C. Chen, J. Hu, D. Shao, J. Li, X. Wang, Adsorption behavior of multiwall carbon nanotube/iron oxide magnetic composites for Ni (II) and Sr (II), J. Hazard. Mater., 164 (2009) 923–928.

[49] F. Unob, B. Wongsiri, N. Phaeon, M. Puanngam, J. Shiowatana, Reuse of waste silica as adsorbent for metal removal by iron oxide modification, J. Hazard. Mater., 142 (2007) 455–462.

[50] W. Konicki, R. Pelka, W. Arabczyk, Adsorption of Ni^{2+} from aqueous solution by magnetic Fe@ graphite nano-composite, Polish J. Chem. Technol., 18 (2016) 96–103.

[51] P.S. Kumar, A. Saravanan, P. Sunder Rajan, M. Yashwanthraj, Nanoscale zero-valent iron-impregnated agricultural waste as an effective biosorbent for the removal of heavy metals from wastewater, Text. Clothing Sustainability, 2 (2016) 1–11.

[52] K. Nithya, A. Sathish, P.S. Kumar, T. Ramachandran, Functional group assisted green synthesized superparamagnetic nanoparticles for the rapid removal of hexavalent chromium from aqueous solution, IET Nanobiotechnol., 11 (2017) 852–860.

[53] P.S. Kumar, R. Gayathri, Adsorption of Pb^{2+} ions from aqueous solutions onto bael tree leaf powder: isotherms, kinetics and thermodynamics study, J. Eng. Sci. Technol., 4 (2009) 381–399.

[54] P.S. Kumar, H. Ethiraj, A. Venkat, N. Deepika, S. Nivedha, T. Vidhyadevi, L. Ravikumar, S. Sivanesan, Adsorption kinetic, equilibrium and thermodynamic investigations of Zn(II) and Ni(II) ions removal by poly(azomethinethioamide) resin with pendent chlorobenzylidine ring, Polish J. Chem. Technol., 17 (2015) 29–38.

[55] K. Nithya, A. Sathish, P.S. Kumar, T. Ramachandran, Biosorption of hexavalent chromium from aqueous solution using raw and acid-treated biosorbent prepared from *Lantana camara* fruit, Desal. Wat. Treat., 57 (2016) 25097–25113.

[56] S. Suganya, A. Saravanan, P.S. Kumar, M. Yashwanthraj, P. Sunder Rajan, K. Kayalvizhi, Sequestration of Pb(II) and Ni(II) ions from aqueous solution using microalga *Rhizoclonium hookeri*: adsorption thermodynamics, kinetics and equilibrium studies, J. Water Reuse Desal., 7 (2017) 214–227.

[57] P.S. Kumar, V.S.S. Bala, K. Ramakrishnan, P. Vijayalakshmi, S. Sivanesan, Kinetics and equilibrium studies of copper removal from aqueous solution by commercial granulated activated carbon, Russ. Chem. Bull., 59 (2010) 1859–1864.

[58] V. Srivastava, C.H. Weng, V.K. Singh, Y.C. Sharma, Adsorption of nickel ions from aqueous solutions by nano alumina: kinetic, mass transfer, and equilibrium studies, J. Chem. Eng. Data, 56 (2011) 1414–1422.

[59] P.S. Kumar, S. Ramalingam, S.D. Kirupha, A. Murugesan, T. Vidhyadevi, S. Sivanesan, Adsorption behavior of Nickel(II) onto cashew nut shell: equilibrium, thermodynamics, kinetics, mechanism and process design, Chem. Eng. J., 167 (2011) 122–131.

[60] U.P. Kiruba, P.S. Kumar, K.S. Gayatri, S.S. Hameed, M. Sindhuja, C. Prabhakaran, Study of adsorption kinetic, mechanism, isotherm, thermodynamic, and design models for Cu(II) ions on sulfuric acid-modified Eucalyptus seeds: temperature effect, Desal. Wat. Treat., 56 (2015) 2948–2965.

[61] A. Saravanan, P.S. Kumar, A.A. Renita, Hybrid synthesis of novel material through acid modification followed ultrasonication to improve adsorption capacity for zinc removal, J. Clean. Prod., 172 (2018) 93–105.

[62] D. Prabu, R. Parthiban, P.S. Kumar, N. Kumari, P. Saikia, Adsorption of copper ions onto nano scale zero-valent iron impregnated cashew nut shell, Desal. Wat. Treat., 57 (2016) 6487–6502.

[63] A. Saravanan, P.S. Kumar, C.F. Carolin, S. Sivanesan, Enhanced adsorption capacity of biomass through ultrasonication for the removal of toxic cadmium ions from aquatic system: temperature influence on isotherms and kinetics, J. Hazard. Toxic Radioactive Waste, 21 (2017) 1–24.

[64] P.S. Kumar, S. Ramakrishnan, S.D. Kirupha, S. Sivanesan, Thermodynamic and kinetic studies of cadmium adsorption from aqueous solution onto rice husk, Braz. J. Chem. Eng., 27 (2010) 347–355.

[65] J. Hu, G. Chen, I.M.C. Lo, Selective removal of heavy metals from industrial wastewater using maghemite nanoparticle: performance and mechanisms, J. Environ. Eng., 132 (2006) 709–715.